Chemical Science

ROYAL SOCIETY OF CHEMISTRY

EDGE ARTICLE

View Article Online
View Journal | View Issue

Cite this: *Chem. Sci.*, 2024, **15**, 16300

All publication charges for this article have been paid for by the Royal Society of Chemistry

An anthracene-containing crown ether: synthesis, host–guest properties and modulation of solid state luminescence†

Weijie Zhu,‡*[abc] Bohan Zhao,‡[a] Shuai Fang,[a] Huangtianzhi Zhu *[a] and Feihe Huang *[ab]

Received 30th July 2024
Accepted 4th September 2024

DOI: 10.1039/d4sc05077k

rsc.li/chemical-science

Organic solid state vapochromic materials are of great significance for the development of supramolecular chemistry and materials science. Herein, we synthesize a crown ether derivative (**An34C10**) containing two anthracene units and construct new crown ether-based vapochromic host–guest co-crystals. Due to the presence of anthracene, **An34C10** not only shows good fluorescence properties but also displays mechanochromism. Single crystal structural analysis, powder X-ray diffraction and differential scanning calorimetry experiments demonstrate that the transformation between different stacking modes of **An34C10** is responsible for mechanochromism. In addition, **An34C10** can complex with 1,2,4,5-tetracyanobenzene (**TCNB**) to form host–guest complex (**An34C10@TCNB**) co-crystals. Because organic solvent fuming alters charge-transfer interactions in **An34C10@TCNB**, the fluorescence of the co-crystals can be turned on and off by 4-methylpyridine and chloroform vapors, respectively, realizing selective detection with opposite emission outputs. Meanwhile, the stimuli-responsive properties of **An34C10** and **An34C10@TCNB** possess good cycling performance. This work provides a new strategy for the construction of organic solid state luminescent materials.

Introduction

Organic solid state vapochromic materials have attracted considerable attention from scientists because of their wide applications in chemical sensors, light-emitting diodes, environmental monitors, and other fields.[1–9] In particular, for molecules containing donor–acceptor structures, their luminescence can be regulated by certain gases such as volatile organic compounds (VOCs), leading to functions in smart devices.[10–14] Such organic donor–acceptor structures usually require tedious synthesis, and molecules with a large degree of conjugation are commonly less stable.[15,16] Therefore, it is urgent to develop new vapochromic materials with simple synthesis and robustness.

Crystal engineering provides a feasible way for preparing crystalline functional materials.[17–28] Owing to solid state complexation upon crystallization, organic host–guest complex co-crystals are promising candidates for robust luminescent materials.[29,30] During co-crystallization, both the donor and acceptor, as the host or guest, respectively, can be included in one system *via* host–guest binding, avoiding tedious covalent synthesis. Meanwhile, compared with the single-component crystalline system, host–guest complex co-crystals show stimuli-responsiveness, leading to more functions, such as molecular ferroelectrics,[31] room-temperature phosphorescence[32–35] and fluorescent devices.[36,37]

As the first generation of macrocycles in supramolecular chemistry, crown ethers have been vigorously studied since they were reported in 1967.[38,39] They have been applied in many fields including supramolecular polymers, supramolecular gels, molecular machines, detection and sensing.[40–54] In general, guests of crown ethers are cationic compounds, such as alkali metal ions and dialkylammonium salts.[55,56] These guests cannot be vaporized under mild conditions, and thus it is difficult to realize vapochromic behaviors based on crown ether-based host–guest complexes. We anticipate that new applications related to vapochromism could be achieved by introducing luminescent crown ethers as hosts.

[a]*Department of Chemistry, Stoddart Institute of Molecular Science, Zhejiang University, Hangzhou 310058, P. R. China. E-mail: htzzhu@zju.edu.cn; fhuang@zju.edu.cn; Fax: (+86) 571-87953189*

[b]*Zhejiang-Israel Joint Laboratory of Self-Assembling Functional Materials, ZJU-Hangzhou Global Scientific and Technological Innovation Center, Hangzhou, 311215, P. R. China*

[c]*School of Chemical and Environmental Engineering, Hunan Institute of Technology, Hengyang 421002, P. R. China. E-mail: weijiezhu@zju.edu.cn*

† Electronic supplementary information (ESI) available: NMR spectra, mass spectra, FT-IR spectra, TGA data, DSC data, PXRD data, crystallographic data, photophysical data, and other materials. CCDC 2226677 and 2226678. For ESI and crystallographic data in CIF or other electronic format see DOI: https://doi.org/10.1039/d4sc05077k

‡ Weijie Zhu and Bohan Zhao contributed equally to this work.

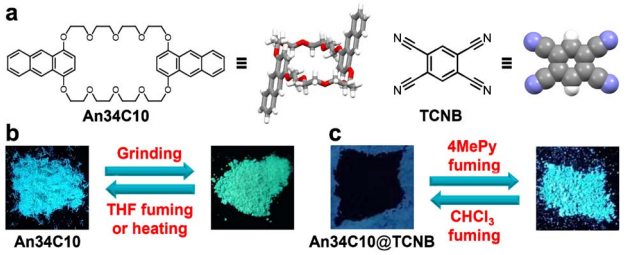

Fig. 1 (a) Chemical structures of An34C10 and TCNB. Schematic representations of (b) An34C10 and (c) An34C10@TCNB under different external stimuli.

In this work, we prepared an anthracene-containing crown ether derivative (**An34C10**) and used it to construct new crown ether-based vapochromic host–guest co-crystals (Fig. 1). Due to the presence of anthracene groups, **An34C10** exhibited intense blue fluorescence emission and mechanochromism. When **An34C10** was ground vigorously in a mortar for several minutes, the emission color changed from blue to yellow-green. After fuming with organic solvents or heating, the fluorescence of the ground sample recovered to the initial blue emission. Furthermore, as the host is a good electron-donor, 1,2,4,5-tetracyanobenzene (**TCNB**) was chosen as the acceptor to form host–guest complex (**An34C10@TCNB**) co-crystals. Although the emission of the co-crystals was quenched by strong charge-transfer (CT), the emission was turned on when the co-crystals were placed in the vapor of 4-methylpyridine, realizing sensing of such vapor with high contrast. Subsequent fuming with chloroform vapor was able to turn off the emission, and thus the material could be recycled. The fluorescence turn-on and turn-off of **An34C10@TCNB** showed excellent robustness and remained unchanged for five cycles.

Results and discussion

The synthetic route to **An34C10** is shown in Fig. S1, ESI†. By using 1,4-anthraquinone and tetraethylene glycol as starting materials, the target macrocycle was finally obtained in a yield of 29% after a five-step reaction.[57–59] All of the new compounds were confirmed by ^{1}H and ^{13}C nuclear magnetic resonance (NMR) and quadrupole-time of flight (Q-TOF) mass spectroscopies (Fig. S2–S9, ESI†).

The photophysical properties of **An34C10** were explored in solution. Fig. S10, ESI† exhibits the absorption spectra of **An34C10** in different solvents. It can be seen that the absorbance of **An34C10** was mainly located between 350 and 450 nm, the characteristic peak of anthracene chromophores.[60] When the solvent polarity increased from hexane to DMSO, the absorption wavelength of **An34C10** displayed a bathochromic shift of about 7 nm. The emission of **An34C10** showed a significant bathochromic shift of 50 nm with the increase of solvent polarity (Fig. S11, ESI†), and the maximum emission peak was red-shifted from 452 nm to 502 nm, indicating that the excited state of **An34C10** was easily polarized compared with the ground state.[60,61]

Anthracene derivatives exhibit photoluminescence not only in solution but also in the solid state.[62] We then explored the solid state emissive properties of **An34C10**. As shown in Fig. 2a, **An34C10** appeared as a yellowish powder under daylight and emitted a bright cyan fluorescence under irradiation of 365 nm UV. According to the solid state photoluminescence (PL) spectra (Fig. 2a and b), the maximum emission peak of **An34C10** was located at 470 nm with a fluorescence lifetime of 2.96 ns. No long-lived emission was observed. We also determined the fluorescence quantum yield (QY) of **An34C10**, which was 13%.

We next investigated the mechanochromism of **An34C10**.[62,63] As shown in Fig. 1b, when **An34C10** crystals were ground in a mortar for 20 minutes, the luminescent color changed from cyan to yellow-green. The maximum emission of **An34C10** displayed a bathochromic shift from 470 nm to 498 nm after grinding (Fig. 2c), and the CIE coordinates changed from (0.18, 0.29) to (0.24, 0.44) (Fig. 2d). The emission of the ground sample was restored to its initial state after heating at 100 °C for 5 minutes or fuming with THF for 2 hours. As characterized by the PL spectra (Fig. 2c), the maximum emission recovered to 470 nm upon heating and THF fuming, indicating that the mechanochromism of **An34C10** was reversible.

In order to study the mechanism of mechanochromism, we tried to get single crystals of **An34C10**. Slowly evaporating a saturated ethyl acetate solution of **An34C10** at room temperature afforded crystals with bright cyan fluorescence. In the single crystal structure (Fig. 3) of **An34C10**, the distance between two anthracene units in one **An34C10** molecule was 6.532 Å, greatly exceeding the effective distance of aryl stacking.[64] Besides, negligible interactions were observed between two adjacent **An34C10** molecules, demonstrating a relatively loose packing. Therefore, the pristine crystals of **An34C10**

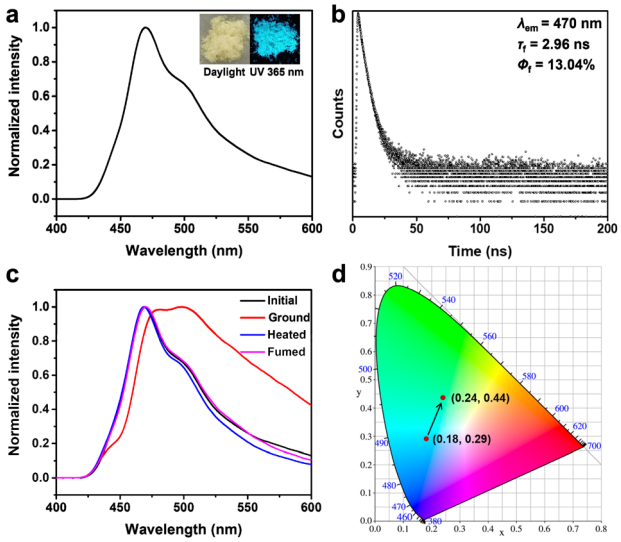

Fig. 2 (a) Normalized fluorescence spectra of An34C10 in the solid state. Insets: pictures of An34C10 under daylight and UV illumination. (b) Emission decay of An34C10 in the solid state. (c) Normalized fluorescence spectra of An34C10 in the solid state under different stimulus conditions. (d) The 1931 CIE coordinate diagram of An34C10 before and after grinding.

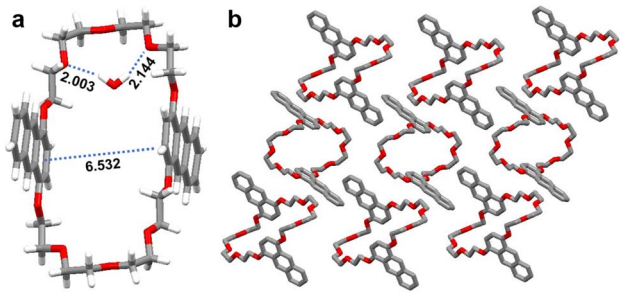

Fig. 3 (a) Single crystal structure of **An34C10**. Carbon atoms are grey, oxygen atoms are red, and hydrogen atoms are white. Crucial distances are marked with dashed lines. One water molecule was encapsulated in the cavity that might come from a trace amount of water in the solvent. Solvent molecules are omitted for clarity. (b) The packing mode of **An34C10**. Hydrogen atoms and solvents are omitted for clarity.

exhibited emission from anthracene monomers. We infer that, upon grinding, the packing mode was partially destroyed (*vide infra*), leading to a relatively dense packing between adjacent anthracene units that further resulted in the bathochromic emission.[60–63] Upon heating or fuming, the dense packing mode became loose again, thus the emission recovered to cyan.

In addition to the single crystal analysis, we also performed ^{1}H NMR, Fourier transform infrared spectroscopy (FT-IR), powder X-ray diffraction (PXRD) and differential scanning calorimetry (DSC) experiments for **An34C10** under different conditions. As can be seen from Fig. S12 and S13, ESI†, the ^{1}H NMR and FT-IR spectra of **An34C10** didn't change after grinding, heating or solvent fuming, which indicated good chemical stability under these stimuli. The PXRD patterns revealed that **An34C10** in the initial state exhibited strong and sharp diffraction peaks that agreed well with the simulated data derived from the single crystal structure, suggesting a well-ordered molecular arrangement (Fig. S14, ESI†). For the ground sample, however, some of the characteristic peaks disappeared in the PXRD pattern, and the intensity of the diffraction peaks was greatly reduced, indicating that the crystal packing changed from ordered stacking to a disordered state. These analyses implied that the emission change resulted from the altered packing mode of the crystals. In addition, after heating or fuming with THF, the sample exhibited restored PXRD diffraction peaks and intensities, and the patterns were consistent with those of the pristine material, indicating that the molecular arrangement of **An34C10** became ordered again.

Then we conducted thermal analysis. DSC curves revealed that the crystalline sample of **An34C10** only exhibited an endothermic peak at about 138 °C, belonging to the melting point (Fig. S15, ESI†). No other phase transition was observed. However, ground **An34C10** displayed two signals in DSC curves. The first one was an exothermic peak located at about 57 °C, which was attributed to the phase transition process, and the other was a melting peak located at about 138 °C. Heating the ground sample for 5 minutes produced an identical DSC curve to that of the pristine material. A similar result was also obtained with the solvent-fumed sample, which only gave a minor difference at about 69 °C on account of solvent loss. Based on the above analysis, it can be inferred that the transformations between packing modes of the **An34C10** crystal are responsible for its reversible mechanochromism.[65] Grinding the crystals produced a metastable dense stacking state, rendering the emission bathochromic shifted. Stimuli such as heating or solvent fuming transformed the unstable dense packing state to the thermodynamically stable crystalline state, which restored the initial emission.

Cycling performance is an important parameter to evaluate the reversibility of mechanochromism, so alternative grinding-heating and grinding-solvent fuming experiments were carried out. As expected, the fluorescence of **An34C10** could be altered between cyan and yellow-green five times without any performance loss, indicating the excellent reversibility of mechanochromism of **An34C10** (Fig. S16 and S17, ESI†).

Considering that **An34C10** is electron-rich, we next investigated the construction of donor–acceptor co-crystals with 1,2,4,5-tetracyanobenzene (**TCNB**) as an electron-deficient guest. We determined the binding stoichiometry of **An34C10** and **TCNB** using the Job's plot, and as expected, the ratio of the host and guest was 1 : 1 (Fig. S18, ESI†). Next, the host–guest recognition between **An34C10** and **TCNB** in solution was investigated by ^{1}H NMR. As shown in Fig. 4a–c, compared with the spectrum of free **TCNB**, upfield shifts occurred for the signal related to proton H_a of **TCNB** in the presence of 1.00 equiv. of **An34C10**. Meanwhile, the proton resonances H_1 and H_2 on

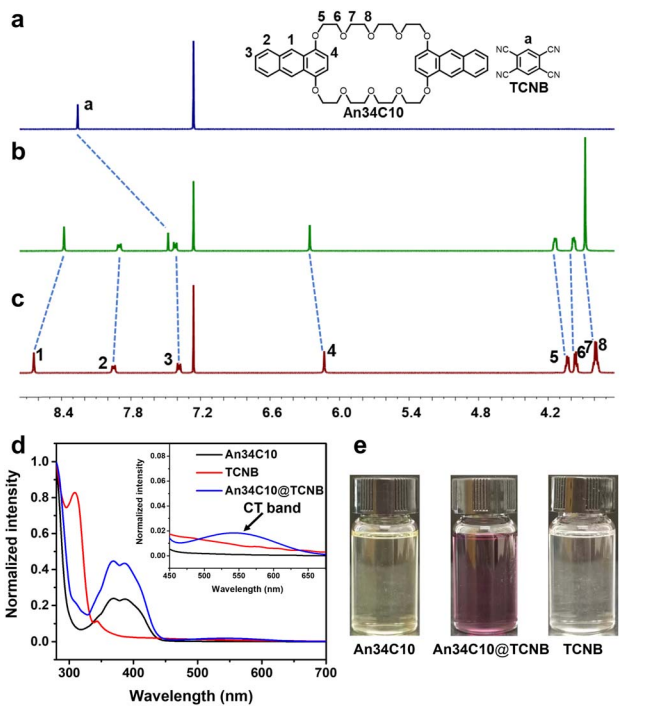

Fig. 4 ^{1}H NMR spectra (400 MHz, chloroform-*d*, 298 K): (a) **TCNB**; (b) 5.00 mM **TCNB** and 5.00 mM **An34C10**; (c) **An34C10**. (d) Normalized UV-vis absorption spectra ($CHCl_3$): **An34C10** (1.00 mM); **TCNB** (1.00 mM); **An34C10** and **TCNB** (1.00 mM, each). (e) Photographs: **An34C10** (1.00 mM); **TCNB** (1.00 mM); **An34C10** and **TCNB** (1.00 mM, each).

An34C10 exhibited upfield shifts and H_3–H_8 shifted downfield upon complexation. These results suggested that **TCNB** was encapsulated in the cavity of **An34C10**, allowing the protons on **TCNB** to be shielded by the electron-rich host. The complexation was also supported by 2D nuclear Overhauser effect spectroscopy (NOESY). Strong correlations between H_a on **TCNB** and H_1 and H_2 on **An34C10** were observed, and thus the guest was located in the cavity of **An34C10** (Fig. S19, ESI†).

We further studied the host–guest complexation between **An34C10** and **TCNB** through UV-vis spectroscopy. As shown in Fig. 4e, after mixing colorless **TCNB** and the light yellow **An34C10** in chloroform, an obvious color change occurred. Different from the UV absorbances of the free host and guest, a new absorption band appeared at about 450–650 nm for the mixed solution ascribed to CT between the host and guest (Fig. 4d). In addition, fluorescence titration experiments were performed to afford the binding constant between **An34C10** and **TCNB** in chloroform. It was found that the color of the solution became darker and the fluorescence intensity decreased during the titration of the guest (Fig. S20, ESI†). The association constant was determined to be $(2.34 \pm 0.12) \times 10^3\ M^{-1}$ by nonlinear fitting in a 1 : 1 complexation mode (Fig. S21, ESI†). Meanwhile, the binding affinity of the host–guest complexation was also investigated by ^{1}H NMR titration experiments (Fig. S22, ESI†). And the association constant was determined to be $(1.91 \pm 0.17) \times 10^3\ M^{-1}$ (Fig. S23, ESI†). The above results revealed strong intermolecular CT interactions between **An34C10** and **TCNB** in chloroform, which enabled the formation of a stable host–guest complex.

The strong interactions in solution prompted us to explore whether CT existed in the solid state. Evaporating an acetone solution of the host–guest complex afforded dark purple crystals (**An34C10@TCNB**) suitable for X-ray single crystal diffraction (Fig. 5). In the single crystal structure, **TCNB** was located in the cavity of **An34C10**, in line with the above spectroscopic results in solution. The guest was stabilized by multiple C–H···N and C–H···O hydrogen bonds, where the distances were 2.849 Å, 3.147 Å, 3.255 Å and 3.284 Å, respectively. Additionally, strong aryl stackings between **An34C10** and **TCNB** with distances of 3.427 Å and 3.439 Å evidenced CT between the host and the guest in the co-crystals. PXRD experiments were performed to analyze the stacking mode of co-crystals. As shown in Fig. S24, ESI†, **An34C10@TCNB** co-crystals showed different PXRD patterns from those of free **An34C10** and **TCNB**, demonstrating that the initial molecular packing modes of single components vanished. In addition, the existence of CT in **An34C10@TCNB** was also confirmed by FT-IR spectroscopy (Fig. S25, ESI†) and thermogravimetric analysis (TGA) (Fig. S26, ESI†).

Then photophysical properties of the co-crystals were explored to further confirm the existence of intermolecular CT. Fig. 6a displays the solid state UV-vis absorption spectrum of **An34C10@TCNB**. A new absorbance appeared at 500–700 nm in the co-crystals that could be attributed to intermolecular CT. In addition, the PL spectrum of **An34C10@TCNB** co-crystals revealed that the host–guest complex was nearly non-emissive (Fig. 6b). This was because the strong intermolecular CT

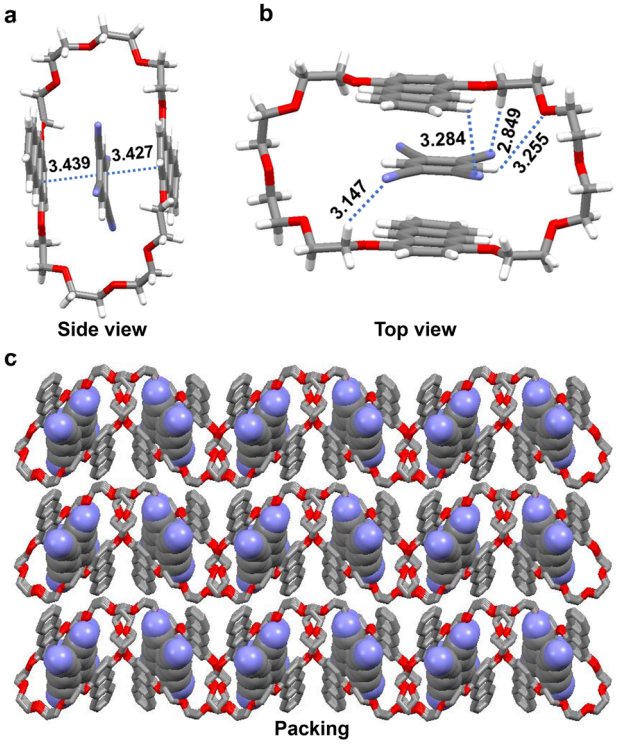

Fig. 5 Single crystal structure of An34C10@TCNB: (a) side view; (b) top view. Carbon atoms are grey, oxygen atoms are red, nitrogen atoms are blue, and hydrogen atoms are white. Crucial distances are marked with dashed lines. Solvents are omitted for clarity. (c) The packing mode of An34C10@TCNB. Hydrogen atoms and solvent molecules are omitted for clarity.

between the host and the guest generated dark states that quenched the emission.[66]

Intermolecular CT is vulnerable to surrounding environments, we thus envisaged that external stimuli could be applied to restore the emission. After screening VOCs, we found that fuming the co-crystals with 4-methylpyridine (**4MePy**) vapor was an effective method to turn on the emission. That is, when **An34C10@TCNB** co-crystals were placed in a saturated atmosphere of **4MePy** vapor for 3 days, the fluorescence of the material recovered. The ^{1}H NMR spectrum of a solution of the fumed co-crystals (denoted as **An34C10@TCNB-4MePy**, Fig. S27, ESI†) illustrated that **4MePy** was trapped in the co-crystals. Besides, the proton signal of **TCNB** showed a slight

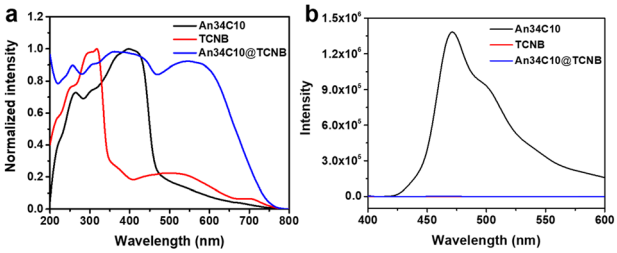

Fig. 6 (a) Normalized solid state UV-vis absorption spectra and (b) fluorescence spectra of An34C10, TCNB and An34C10@TCNB.

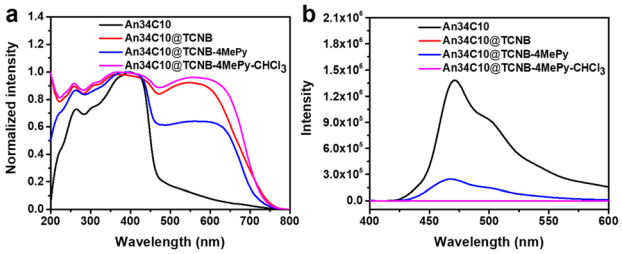

Fig. 7 (a) Normalized solid state UV-vis absorption spectra and (b) solid state fluorescence spectra of An34C10, An34C10@TCNB, An34C10@TCNB-4MePy and An34C10@TCNB-4MePy-$CHCl_3$.

downfield shift compared with that of **An34C10@TCNB** (Fig. S28, ESI†), evidencing weakened CT interactions that turned on the emission of the host. Such turn-on emission clearly indicates that the co-crystal is a promising candidate for sensing and detection of pyridyl compounds.

TGA also confirmed the existence of three components (Fig. S29, ESI†). Three plateaus were observed in the thermogravimetric curve of **An34C10@TCNB-4MePy**. The first plateau implied the desorption of solvent molecules, that is, **4MePy**. The amount of **4MePy** adsorbed by co-crystals was determined to be 0.89 molecules per host–guest complex, in good agreement with the results of the ^{1}H NMR spectrum. The latter two plateaus corresponded to the decompositions of **TCNB** and **An34C10**, respectively. Similarly, the photophysical properties of **An34C10@TCNB-4MePy** were characterized. The solid state UV-vis spectrum showed a decrease in the CT band compared with that of **An34C10@TCNB** (Fig. 7a). The PL spectrum of **An34C10@TCNB-4MePy** was the same as that of **An34C10**, indicating that the fluorescence came from the luminescence of the macrocycle (Fig. 7b). However, the luminescence intensity was greatly reduced, and the fluorescence quantum yield was determined to be 1.9%. PXRD patterns revealed that after **4MePy** fuming, some of the diffraction signals corresponded well to those of the macrocycle (Fig. S30, ESI†). These results confirmed that **4MePy** fuming weakened CT interactions in the co-crystal, thus enabling the fluorescence of **An34C10** to turn on again. Besides, when **An34C10@TCNB** was exposed to other common VOC vapors such as toluene, cyclohexane, methylcyclohexane, pyridine, 2-methylpyridine, and 3-methylpyridine at room temperature, no fluorescence was observed (Fig. S31, ESI†). The main diffraction peaks in PXRD patterns and fluorescence spectra of **An34C10@TCNB** did not change after absorption of these VOCs, which exhibited the selective vapochromic behaviors for **4MePy** (Fig. S32 and S33, ESI†).

Although crystallization of **An34C10**, **TCNB**, and **4MePy** failed, we still observed that when **An34C10@TCNB** co-crystals were immersed in a 1.0 mol L^{-1} **4MePy** aqueous solution for 10 days (Fig. S34, ESI†), light yellow cracks appeared on the surfaces of the dark purple crystals. These cracks emitted blue fluorescence under 365 nm UV irradiation, which is consistent with the induced emission in the presence of **4MePy**.

Additionally, it was found that when **An34C10@TCNB-4MePy** was placed in chloroform vapor, the fluorescence of the material was quickly quenched (denoted as **An34C10@TCNB-4MePy-$CHCl_3$**, Fig. 7b). PXRD experiments (Fig. S30, ESI†) showed that the pattern after fuming with chloroform was consistent with that of **An34C10@TCNB**, indicating that the crystal structure was restored to the initial CT state. This implied that chloroform could be a competitive guest, whereby **4MePy** is released and the co-crystals become non-emissive again. However, under vapors of other haloalkanes and aryl halides, such as tetrachloromethane, 1-iodobutane, 1,4-dibromobutane, chlorobenzene and bromobenzene, the fluorescence of **An34C10@TCNB-4MePy** remained unchanged (Fig. S35 and S36, ESI†). And the main PXRD diffractions of crystals after vapor exposure were consistent with those before fuming (Fig. S37, ESI†). These results showed that **An34C10@TCNB-4MePy** displayed a high selectivity for chloroform vapor.

Moreover, we tested the recyclability of the vapochromic behaviors for **An34C10@TCNB** (Fig. S38, ESI†). As expected, after alternative fuming with **4MePy** and chloroform vapors, the fluorescence of **An34C10@TCNB** could be switched between on and off at least five times without any performance loss, which indicated the good cycling performance of host–guest co-crystals. The on and off switches hold potential in the fabrication of smart luminescent materials with response to pyridyl and alkyl chloride compounds.

Conclusions

In summary, we synthesized a crown ether derivative containing two anthracene units and investigated the host–guest co-crystals based on crown ether for vapochromism. Due to the presence of anthracene, **An34C10** not only emitted bright blue fluorescence, but also showed mechanochromic properties, and the fluorescence change could be recovered by heating or organic solvent fuming. Through various experimental analyses, it was found that the mechanochromism of **An34C10** was derived from a transition between different stacking structures. In addition, **An34C10** complexes with **TCNB** to form co-crystals. Due to the strong charge-transfer interactions between the host and guest, the fluorescence was quenched. Since solvent fuming would weaken intermolecular charge-transfer interactions, the fluorescence of co-crystals was turned on by fuming with **4MePy**. Interestingly, when the emissive co-crystal was further fumed with chloroform vapor, the fluorescence was quenched again, and the structure of co-crystals returned to the initial state. Meanwhile, both the mechanochromism of **An34C10** and the fluorescence turn-on and off in **An34C10@TCNB** displayed good cycling performance. This work not only broadens the application of supramolecular chemistry but also combines a macrocycle with co-crystal engineering, providing a new strategy for the preparation of various stimuli-responsive crystalline materials.

Data availability

The crystallographic data for **An34C10** and **An34C10@TCNB** have been deposited at CCDC with deposition numbers 2226677 and 2226678, respectively. The data can be obtained *via*

https://www.ccdc.cam.ac.uk/structures. Data for this paper, including synthesis and structural characterizations, are available in the ESI.† The raw data are available from the authors upon reasonable request.

Author contributions

W. Zhu, H. Zhu and F. Huang proposed the project and designed the study. W. Zhu and B. Zhao performed the experiments. W. Zhu, S. Fang and H. Zhu analyzed the data. W. Zhu, H. Zhu and F. Huang wrote the manuscript with inputs from all authors. F. Huang directed the project with critical consultation from H. Zhu.

Conflicts of interest

There are no conflicts to declare.

Acknowledgements

This work was supported by National Key Research and Development Program of China (2021YFA0910100), National Natural Science Foundation of China (22035006, 22320102001, and 22350007), Zhejiang Provincial Natural Science Foundation of China (LD21B020001), the Starry Night Science Fund of Zhejiang University Shanghai Institute for Advanced Study (SN-ZJU-SIAS-006), and the Leading Innovation Team grant from Department of Science and Technology of Zhejiang Province (2022R01005). We thank The Chemistry Instrumentation Center of Zhejiang University and The Instrumentation and Service Center for Molecular Sciences at Westlake University for the technical support.

Notes and references

1 X. Zhang, B. Li, Z.-H. Chen and Z.-N. Chen, *J. Mater. Chem.*, 2012, **22**, 11427–11441.
2 M. H. Keefe, K. D. Benkstein and J. T. Hupp, *Coord. Chem. Rev.*, 2000, **205**, 201–228.
3 E. J. Fernández, A. Laguna and J. M. López-De-Luzuriaga, *Coord. Chem. Rev.*, 2005, **249**, 1423–1433.
4 M. J. Katz, K. Sakai and D. B. Leznoff, *Chem. Soc. Rev.*, 2008, **37**, 1884–1895.
5 Q. Zhao, F. Li and C. Huang, *Chem. Soc. Rev.*, 2010, **39**, 3007–3030.
6 L. You, D. Zha and E. V. Anslyn, *Chem. Rev.*, 2015, **115**, 7840–7892.
7 Y. Sagara, M. Karman, E. Verde-Sesto, K. Matsuo, Y. Kim, N. Tamaoki and C. Weder, *J. Am. Chem. Soc.*, 2018, **140**, 1584–1587.
8 Y. Sagara, H. Traeger, J. Li, Y. Okado, S. Schrettl, N. Tamaoki and C. Weder, *J. Am. Chem. Soc.*, 2021, **143**, 5519–5525.
9 S. Thazhathethil, T. Muramatsu, N. Tamaoki, C. Weder and Y. Sagara, *Angew. Chem., Int. Ed.*, 2022, **61**, e202209225.
10 M.-S. Yuan, D.-E. Wang, P. Xue, W. Wang, J.-C. Wang, Q. Tu, Z. Liu, Y. Liu, Y. Zhang and J. Wang, *Chem. Mater.*, 2014, **26**, 2467–2477.
11 S. H. Lim, M. M. Olmstead and A. L. Balch, *Chem. Sci.*, 2013, **4**, 311–318.
12 S. Ito, *CrystEngComm*, 2022, **24**, 1112–1126.
13 E. Li, K. Jie, Y. Fang, P. Cai and F. Huang, *J. Am. Chem. Soc.*, 2020, **142**, 15560–15568.
14 D. Gentili, M. Gazzano, M. Melucci, D. Jones and M. Cavallini, *Chem. Soc. Rev.*, 2019, **48**, 2502–2517.
15 Y. Im, M. Kim, Y. J. Cho, J.-A. Seo, K. S. Yook and J. Y. Lee, *Chem. Mater.*, 2017, **29**, 1946–1963.
16 B. Kim, G. Storch, G. Banerjee, B. Q. Mercado, J. Castillo-Lora, G. W. Brudvig, J. M. Mayer and S. J. Miller, *J. Am. Chem. Soc.*, 2017, **139**, 15239–15244.
17 G. R. Desiraju, *Angew Chem. Int. Ed. Engl.*, 1995, **34**, 2311–2327.
18 J. J. Wolff, *Angew Chem. Int. Ed. Engl.*, 1996, **35**, 2195–2197.
19 H. Yamagishi, H. Sato, A. Hori, Y. Sato, R. Matsuda, K. Kato and T. Aida, *Science*, 2018, **361**, 1242–1246.
20 M. Irie, T. Fukaminato, K. Matsuda and S. Kobatake, *Chem. Rev.*, 2014, **114**, 12174–12277.
21 A. G. Slater, M. A. Little, A. Pulido, S. Y. Chong, D. Holden, L. Chen, C. Morgan, X. Wu, G. Cheng, R. Clowes, M. E. Briggs, T. Hasell, K. E. Jelfs, G. M. Day and A. I. Cooper, *Nat. Chem.*, 2017, **9**, 17–25.
22 G. Li, Z. Zhou, C. Yuan, Z. Guo, Y. Liu, D. Zhao, K. Liu, J. Zhao, H. Tan and X. Yan, *Angew. Chem., Int. Ed.*, 2020, **59**, 10013–10017.
23 K. Gao, Q. Feng, Z. Zhang, R. Zhang, Y. Hou, C. Mu, X. Li and M. Zhang, *Angew. Chem., Int. Ed.*, 2022, **61**, e202209958.
24 K. Wang, S. Huang, Y. Zhang, S. Zhao, H. Zhang and Y. Wang, *Chem. Sci.*, 2013, **4**, 3288–3293.
25 H. Xia, D. Liu, K. Song and Q. Miao, *Chem. Sci.*, 2011, **2**, 2402–2406.
26 Z. Li, Y. Han, F. Nie, M. Liu, H. Zhong and F. Wang, *Angew. Chem., Int. Ed.*, 2021, **60**, 8212–8219.
27 B. Li, L. Cui and C. Li, *Angew. Chem., Int. Ed.*, 2020, **59**, 22012–22016.
28 M. Wang, Q. Li, E. Li, J. Liu, J. Zhou and F. Huang, *Angew. Chem., Int. Ed.*, 2021, **60**, 8115–8120.
29 H. Zhu, L. Chen, B. Sun, M. Wang, H. Li, J. F. Stoddart and F. Huang, *Nat. Rev. Chem*, 2023, **7**, 768–782.
30 L. Sun, Y. Wang, F. Yang, X. Zhang and W. Hu, *Adv. Mater.*, 2019, **31**, 1902328–1902349.
31 X.-J. Song, T. Zhang, Z.-X. Gu, Z.-X. Zhang, D.-W. Fu, X.-G. Chen, H.-Y. Zhang and R.-G. Xiong, *J. Am. Chem. Soc.*, 2021, **143**, 5091–5098.
32 W.-L. Zhou, W. Lin, Y. Chen and Y. Liu, *Chem. Sci.*, 2022, **13**, 7976–7989.
33 Z.-Y. Zhang and Y. Liu, *Chem. Sci.*, 2019, **10**, 7773–7778.
34 Y. Sun, L. Jiang, L. Liu, Y. Chen, W.-W. Xu, J. Niu, Y. Qin, X. Xu and Y. Liu, *Adv. Opt. Mater.*, 2023, **11**, 2300326–2300334.
35 Y. Zhao, B. Ding, Z. Huang and X. Ma, *Chem. Sci.*, 2022, **13**, 8412–8416.
36 B. Hua, W. Zhou, Z. Yang, Z. Zhang, L. Shao, H. Zhu and F. Huang, *J. Am. Chem. Soc.*, 2018, **140**, 15651–15654.

37 B. Hua, C. Zhang, W. Zhou, L. Shao, Z. Wang, L. Wang, H. Zhu and F. Huang, *J. Am. Chem. Soc.*, 2020, **142**, 16557–16561.
38 C. J. Pedersen, *J. Am. Chem. Soc.*, 1967, **89**, 2495–2496.
39 R. M. Izatt, *Chem. Soc. Rev.*, 2017, **46**, 2380–2384.
40 G. W. Gokel, W. M. Leevy and M. E. Weber, *Chem. Rev.*, 2004, **104**, 2723–2750.
41 B. Zheng, F. Wang, S. Dong and F. Huang, *Chem. Soc. Rev.*, 2012, **41**, 1621–1636.
42 Z. Liu, S. K. M. Nalluri and J. F. Stoddart, *Chem. Soc. Rev.*, 2017, **46**, 2459–2478.
43 E. Li, K. Jie, M. Liu, X. Sheng, W. Zhu and F. Huang, *Chem. Soc. Rev.*, 2020, **49**, 1517–1544.
44 A. Dhara, A. Dmitrienko, R. N. N. Hussein, A. Sotomayor, B. H. H. Wilson and S. J. J. Loeb, *Chem. Sci.*, 2023, **14**, 7215–7220.
45 C.-H. Wang, K.-J. Chen, T.-H. Wu, H.-K. Chang, Y. Tsuchido, Y. Sei, P.-L. Chen and M. Horie, *Chem. Sci.*, 2021, **12**, 3871–3875.
46 A. Aster, G. Licari, F. Zinna, E. Brun, T. Kumpulainen, E. Tajkhorshid, J. Lacour and E. Vauthey, *Chem. Sci.*, 2019, **10**, 10629–10639.
47 Z. Niu and H. W. Gibson, *Chem. Rev.*, 2009, **109**, 6024–6046.
48 M. Lee, R. B. Moore and H. W. Gibson, *Macromolecules*, 2011, **44**, 5987–5993.
49 A. Aydogan, D. J. Coady, S. K. Kim, A. Akar, C. W. Bielawski, M. Marquez and J. L. Sessler, *Angew. Chem., Int. Ed.*, 2008, **47**, 9648–9652.
50 O. A. Fedorova, E. Y. Chernikova, Y. V. Fedorov, E. N. Gulakova, A. S. Peregudov, K. A. Lyssenko, G. Jonusauskas and L. Isaacs, *J. Phys. Chem. B*, 2009, **113**, 10149–10158.
51 R. Saha, B. Mondal and P. S. Mukherjee, *Chem. Rev.*, 2022, **122**, 12244–12307.
52 R. Kumar, A. Sharma, H. Singh, P. Suating, H. S. Kim, K. Sunwoo, I. Shim, B. C. Gibb and J. S. Kim, *Chem. Rev.*, 2019, **119**, 9657–9721.
53 D. Zhao, Z. Zhang, J. Zhao, K. Liu, Y. Liu, G. Li, X. Zhang, R. Bai, X. Yang and X. Yan, *Angew. Chem., Int. Ed.*, 2021, **60**, 16224–16229.
54 P. Wei, X. Zhang, J. Liu, G.-G. Shan, H. Zhang, J. Qi, W. Zhao, H. H.-Y. Sung, I. D. Williams, J. W. Y. Lam and B. Z. Tang, *Angew. Chem., Int. Ed.*, 2020, **59**, 9293–9298.
55 C. Zhang, S. Li, J. Zhang, K. Zhu, N. Li and F. Huang, *Org. Lett.*, 2007, **9**, 5553–5556.
56 X. Ji, Y. Yao, J. Li, X. Yan and F. Huang, *J. Am. Chem. Soc.*, 2013, **135**, 74–77.
57 S. Murkli, J. Klemm, D. King, P. Y. Zavalij and L. Isaacs, *Chem.–Eur. J.*, 2020, **26**, 15249–15258.
58 E. Chirkin, V. Muthusamy, P. Mann, T. Roemer, P. G. Nantermet and D. A. Spiegel, *Angew. Chem., Int. Ed.*, 2017, **56**, 13036–13040.
59 Y.-L. Zhao, L. Liu, W. Zhang, C.-H. Sue, Q. Li, O. Š. Miljanić, O. M. Yaghi and J. F. Stoddart, *Chem.–Eur. J.*, 2009, **15**, 13356–13380.
60 Q. Dai, J. Zhang, R. Tan, S. Wang, Y. Li, Q. Li and S. Xiao, *Mater. Lett.*, 2016, **164**, 239–242.
61 R. Li, S. Xiao, Y. Li, Q. Lin, R. Zhang, J. Zhao, C. Yang, K. Zou, D. Li and T. Yi, *Chem. Sci.*, 2014, **5**, 3922–3928.
62 K. C. Naeem, A. Subhakumari, S. Varughese and V. C. Nair, *J. Mater. Chem. C*, 2015, **3**, 10225–10231.
63 K. Duraimurugan, M. Harikrishnan, J. Madhavan, A. Siva, S. J. Lee, J. Theerthagiri and M. Y. Choi, *Environ. Res.*, 2021, **194**, 110741–110748.
64 C. Janiak, *J. Chem. Soc. Dalton Trans.*, 2000, **21**, 3885–3896.
65 X. Zhang, Z. Chi, X. Zhou, S. Liu, Y. Zhang and J. Xu, *J. Phys. Chem. C*, 2012, **116**, 23629–23638.
66 H. Zhu, J. Liu, Y. Wu, L. Wang, H. Zhang, Q. Li, H. Wang, H. Xing, J. L. Sessler and F. Huang, *J. Am. Chem. Soc.*, 2023, **145**, 11130–11139.